Available online at www.sciencedirect.com
ScienceDirect
Finite Elements in Analysis and Design 43 (2007) 1169–1178
FINITE ELEMENTS IN ANALYSIS AND DESIGN
www.elsevier.com/locate/finel

Peridynamics via finite element analysis

Richard W. Macek[a,*], Stewart A. Silling[b]

[a]WT-1, MS P946, Los Alamos National Laboratory, P.O. Box 1663, Los Alamos, NM 87545, USA
[b]Sandia National Laboratories, New Mexico, P.O. Box 5800, Albuquerque, NM 87185-(1322), USA

Received 30 January 2007; received in revised form 10 July 2007; accepted 21 August 2007
Available online 23 October 2007

Abstract

Peridynamics is a recently developed theory of solid mechanics that replaces the partial differential equations of the classical continuum theory with integral equations. Since the integral equations remain valid in the presence of discontinuities such as cracks, the method has the potential to model fracture and damage with great generality and without the complications of mathematical singularities that plague conventional continuum approaches. Although a discretized form of the peridynamic integral equations has been implemented in a meshless code called EMU, the objective of the present paper is to describe how the peridynamic model can also be implemented in a conventional finite element analysis (FEA) code using truss elements. Since FEA is arguably the most widely used tool for structural analysis, this implementation may hasten the verification of peridynamics and significantly broaden the range of problems that the practicing analyst might attempt. Also, the present work demonstrates that different subregions of a model can be solved with either the classical partial differential equations or the peridynamic equations in the same calculation thus combining the efficiency of FEA with the generality of peridynamics. Several example problems show the equivalency of the FEA and the meshless peridynamic approach as well as demonstrate the utility and robustness of the method for problems involving fracture, damage and penetration.
Published by Elsevier B.V.

Keywords: Peridynamics; Finite; Element; Penetration; Fracture; Damage

1. Introduction

Numerical prediction of crack growth and damage are long-standing problems in computational mechanics. The difficulties inherent in these problems arise from the basic incompatibility of cracks with the partial differential equations that are used in the classical theory of solid mechanics. The spatial derivatives needed for these partial differential equations to make sense do not exist on a crack tip or surface. Therefore, any numerical method derived from these equations inherits this difficulty in modeling cracks. Typically such methods also require supplemental relations that govern the initiation, as well as the growth velocity and direction, of cracks. These relations must be applied along each crack tip, leading to the inherent complexity of the method, particularly when multiple cracks occur and interact in three dimensions. As an attempt in improving this situation, a theory of solid mechanics has been proposed that does not require spatial derivatives to be evaluated within a body [1–6]. This theory, known as the peridynamic theory, instead uses integral equations. The objective is to reformulate the basic mathematical description of solid mechanics in such a way that the identical equations hold either on or off of a discontinuity such as a crack.

As with any new scientific theory complete validation is a continuous process that may take many years to complete. Therefore, rather than verification of the peridynamic theory, the primary motivation of this paper is to show that the basic peridynamic equations are entirely consistent with even the most fundamental finite element analysis (FEA) code architectures and that within the FEA framework, coupling of peridynamics to conventional FEA models is very possible. For completeness a summary of the peridynamic continuum theory and the principal numerical equations used in the meshless EMU code [7] that implements this continuum model are presented. Several examples demonstrate the equivalency of the FEA and the direct implementations as well as the ease of performing peridynamics in a FEA code. Given the popularity and

* Corresponding author. Tel.: +1 505 667 2229; fax: +1 505 665 2137.
E-mail address: rwmacek@lanl.gov (R.W. Macek).

0168-874X/$ - see front matter Published by Elsevier B.V.
doi:10.1016/j.finel.2007.08.012

utility of FEA, this latter realization may hasten the verification of peridynamics and significantly broaden the range of problems that the practicing structural analyst might undertake.

2. Peridynamic theory for a continuum

In this section we have removed background material that was redundant of our previously published work [1,4], but retained a concise summary of the theory for the convenience of readers.

The peridynamic theory may be thought of as a continuum version of molecular dynamics. Outlining the development detailed in [4], the acceleration of any particle at $\mathbf{x}$ in the reference configuration at time t is found from

$$\rho\ddot{\mathbf{u}}(x,t)=\int_{H_\mathbf{x}} \boldsymbol{f}(\mathbf{u}(\mathbf{x}',t)-\mathbf{u}(\mathbf{x},t),\mathbf{x}'-\mathbf{x})\,\mathrm{d}V_{\mathbf{x}'}+\mathbf{b}(\mathbf{x},t), \quad (1)$$

where H_x is a neighborhood of $\mathbf{x}$ with a horizon radius of δ, $\mathbf{u}$ is the displacement vector field, $\mathbf{b}$ is a prescribed body force density field, ρ is mass density in the reference configuration, and $\boldsymbol{f}$ is a *pairwise force function* whose value is the force vector (per unit volume squared) that the particle $\mathbf{x}'$ exerts on the particle $\mathbf{x}$. Also, the relative position of these two particles in the reference configuration $\boldsymbol{\xi}$ is given by

$$\boldsymbol{\xi}=\mathbf{x}'-\mathbf{x} \quad (2)$$

and their relative displacement by

$$\boldsymbol{\eta}=\mathbf{u}(\mathbf{x}',t)-\mathbf{u}(\mathbf{x},t). \quad (3)$$

Note that $\boldsymbol{\eta}+\boldsymbol{\xi}$ represents the current relative position vector connecting the particles. The direct physical interaction (which occurs through unspecified means) between the particles at $\mathbf{x}$ and $\mathbf{x}'$ is called a *bond*, or in the special case of an elastic interaction, a *spring*. In addition, from Eq. (1) the bonds for any given particle do not extend past the horizon, i.e., particles only interact within the horizon. Indeed, the concept of a bond that extends over a finite distance is a fundamental difference between the peridynamic theory and the classical theory, which is based on the idea of contact forces (interactions between particles that are in direct contact with each other). As with the conventional interpretation of a spring, linear and angular momentum are conserved because the bond forces are equal and opposite and because they are directed along the vector connecting the current positions of any two interacting particles. Extending the development in [4], the general form of the bond force for the basic theory can be written as

$$\boldsymbol{f}(\boldsymbol{\eta},\boldsymbol{\xi})=\frac{\boldsymbol{\xi}+\boldsymbol{\eta}}{|\boldsymbol{\xi}+\boldsymbol{\eta}|}f(y(t),\boldsymbol{\xi},t) \quad \forall\boldsymbol{\xi},\boldsymbol{\eta}, \quad (4)$$

where f is the scalar bond force and

$$y=|\boldsymbol{\eta}+\boldsymbol{\xi}|. \quad (5)$$

Eqs. (1) and (4) constitute the essence of the basic peridynamic continuum theory.

To facilitate development of constitutive models as in [4,7], the scalar bond stretch s is defined as

$$s=\frac{|\boldsymbol{\xi}+\boldsymbol{\eta}|-|\boldsymbol{\xi}|}{|\boldsymbol{\xi}|}=\frac{y-|\boldsymbol{\xi}|}{|\boldsymbol{\xi}|}. \quad (6)$$

For a brittle microelastic material, f takes the form [4]:

$$f(s,t,\boldsymbol{\xi})=\mu(t,\boldsymbol{\xi})=\mu(t,\boldsymbol{\xi})cs, \quad (7)$$

where c is the spring constant and μ is a history dependent damage function that takes on a value of 0 or 1, i.e.,

$$\mu(t,\boldsymbol{\xi})=\begin{cases}1 & \text{if } s(t',\boldsymbol{\xi})<s_0 \quad \forall 0\leqslant t'\leqslant t,\\ 0 & \text{otherwise.}\end{cases} \quad (8)$$

Here, s_0 is the critical bond stretch for failure. Eq. (8) ensures that once a bond has exceeded its failure stretch it is broken or removed from the analysis and is never reintroduced. Damage at a point [4] is defined as

$$\varphi(\mathbf{x},t)=\frac{1-\int_{H_\mathbf{x}}\mu(\mathbf{x},t,\boldsymbol{\xi})\,\mathrm{d}V_\xi}{\int_{H_\mathbf{x}}\mathrm{d}V_\xi}. \quad (9)$$

The value of c corresponding to the classical continuum mechanics bulk modulus k is found by equating the strain energy under isotropic extension from continuum mechanics to the energy density within the horizon in the peridynamic theory for the same deformation. Thus, as in [4]

$$c=\frac{18k}{\pi\delta^4}. \quad (10)$$

In a similar fashion [4] the critical stretch for band failure, s_0, is related to the energy release rate, G_0, by requiring the work to break all the bonds per unit area to equal the energy release rate, thus yielding

$$s_0=\sqrt{\frac{10G_0}{\pi c\delta^5}}=\sqrt{\frac{5G_0}{9k\delta}}. \quad (11)$$

A microplastic material is a material whose bond force takes the form

$$f(s,\boldsymbol{\xi},t)=\begin{cases}c(s-\bar{s}(t)) & \text{if } |\boldsymbol{\xi}|\leqslant\delta,\\ 0 & \text{otherwise,}\end{cases} \quad (12)$$

where

$$\bar{s}(0)=0, \quad \dot{\bar{s}}=\begin{cases}\dot{\bar{s}} & \text{if } |s-\bar{s}|\leqslant s_Y,\\ 0 & \text{otherwise.}\end{cases} \quad (13)$$

At the bond level this material is elastic–perfectly plastic with a yield stretch s_Y and a plastic stretch history $\bar{s}(t)$. However, at the macroscopic or continuum level the material strain hardens because all bonds do not yield at the same time or deformation level. As with the brittle microelastic material, to be useful the bond properties need to be related to measurable macroscopic properties. In this case the bond yield stretch can be related to the engineering ultimate strength (stress) σ_{ult} by noting that all bonds have yielded when the material reaches it ultimate strength. Therefore, paralleling the development in [4] that lead

to the relation for the critical bond stretch in the brittle microelastic material, Eq. (11), one can write

$$\boldsymbol{\sigma}_{\text{ult}} \approx \int_0^{\delta}\int_0^{2\pi}\int_z^{\delta}\int_0^{\cos^{-1} z/\xi} \times f_Y \boldsymbol{\xi}^2 \cos\phi \sin\phi \,\mathrm{d}\phi \,\mathrm{d}\boldsymbol{\xi} \,\mathrm{d}\theta \,\mathrm{d}z = \frac{\pi f_Y \delta^4}{6}, \tag{14}$$

where the bond force at yield f_Y is given by

$$f_Y = c s_Y. \tag{15}$$

The approximation in Eq. (14) arises from the fact that the integration is performed with the undeformed geometry rather than the deformed geometry. Solving Eqs. (10), (14), and (15) for the bond yield stretch produces the following relation between the bond yield stretch and conventional continuum mechanics properties:

$$s_Y \approx \frac{\sigma_{\text{ult}}}{3k}. \tag{16}$$

The models described above allow only one elastic constant, c, whereas isotropic linear elastic materials in the classical theory are characterized by two such constants. This difference occurs because an elastic solid that involves only two-particle interactions (a "Cauchy crystal") always has a Poisson ratio of $\frac{1}{4}$. A refinement of the peridynamic theory that allows dependence of strain energy density on local volume change in addition to two-particle interactions removes this restriction [1] and can be implemented to model fluids. Indeed, allowing the bond properties to depend not only on the stretch in that bond, itself, but also on the stretch of all bonds connected to its end points may permit more general constitutive models in the peridynamic theory. In this paper only the brittle microelastic and the microplastic constitutive models are utilized although even within this framework more elaborate models are certainly possible. For instance, anisotropy can be introduced through the dependence of the bond force on $\boldsymbol{\xi}$.

3. Short-range forces

In the peridynamic theory, particles interact only through bonds. Therefore, particles that are separated in the reference configuration by distances greater than the horizon δ do not interact because of Eq. (1). However, in practice, many applications involve multiple bodies that are initially separated by a large (compared with δ) distance but eventually come into contact. The theory developed so far cannot encompass contact forces.

To allow for contact forces, *short-range* forces are now introduced. These forces do not depend on the distance between particles in the reference configuration, only on their relative position in the current configuration. Specifically, it is assumed that

$$\boldsymbol{f}_s(\mathbf{y}', \mathbf{y}) = \frac{\mathbf{y}' - \mathbf{y}}{|\mathbf{y}' - \mathbf{y}|} \min\left\{0, c_s\left(\frac{|\mathbf{y}' - \mathbf{y}|}{2r_s} - 1\right)\right\}, \tag{17}$$

where c_s and r_s are positive constants, and $\mathbf{y}$ and $\mathbf{y}'$ are the deformed positions of $\mathbf{x}$ and $\mathbf{x}'$, respectively,

$$\mathbf{y} = \mathbf{x} + \mathbf{u}, \quad \mathbf{y}' = \mathbf{x}' + \mathbf{u}'. \tag{18}$$

Thus, short-range forces are nonzero only when the two particles are closer to each other than $2r_s$. For this reason, r_s is called the node radius. Short-range forces can be only compressive (repulsive), according to Eq. (17).

For proportional materials, the value of c_s can be chosen to be some multiple of c, where c is the spring constant of the material. The multiple depends on the desired stiffness of the contact forces. A suitable default, which results in a stiffness close to that of the bulk elastic properties of the material, is

$$c_s = 15c. \tag{19}$$

4. Force normalization at surfaces

It was shown in Eq. (10) that the spring constant can be obtained from the bulk elastic modulus for a real material. However, the derivation that leads to this result assumed that a given material particle has surrounding it a spherical neighborhood of radius δ completely filled with the same material. This assumption does not hold if the particle is within a distance δ of a free surface or an interface with some other material. If the spring constant given by Eq. (10) is used for such points, the resulting body would have incorrect bulk elastic properties.

To account for this effect near free surfaces and interfaces, a correction called force normalization is used. In this method, if $\mathbf{X}$ is a point in the body, possibly near a surface, let the tensor $\mathbf{P}(\mathbf{X})$ be defined by

$$\mathbf{P}(\mathbf{X}) = \frac{\partial}{\partial \mathbf{U}} \int_{H_X} \boldsymbol{f}(\mathbf{U}, \mathbf{X} - \mathbf{x}') \,\mathrm{d}V_{\mathbf{x}'}. \tag{20}$$

Thus, $-\mathbf{P}(\mathbf{X})\Delta\mathbf{u}$ equals the restoring force (per unit volume) that the particle $\mathbf{X}$ experiences if it is displaced incrementally through a small vector $\Delta\mathbf{u}$ while holding all other points fixed. It can be shown that $\mathbf{P}$ is a symmetric tensor [1] that is also positive definite for reasonably behaved materials. Therefore, $\mathbf{P}$ has three positive eigenvalues $\{p^1, p^2, p^3\}$. Let p^1 be the largest of these. Further, let P_∞ be the analogous tensor obtained for a large homogeneous body (in contrast to $\mathbf{P}(\mathbf{X})$, which takes into account the particular location of $\mathbf{X}$). The eigenvalues of $\mathbf{P}_\infty$ are denoted $\{p^1_\infty, p^2_\infty, p^3_\infty\}$, with p^1_∞ being the largest of the three.

Let c_∞ be the spring constant obtained from Eq. (10), i.e., the value appropriate for a large homogeneous body composed of the material that is present at $\mathbf{X}$. Then the modified spring constant $c(\mathbf{X})$, taking into account surfaces and interfaces near point $\mathbf{X}$, is set to

$$c(\mathbf{X}) = \frac{c_\infty p^1_\infty}{p^1(\mathbf{X})}. \tag{21}$$

In general, $c(\mathbf{X}) \geqslant c_\infty$. The assumption in this force normalization method is that the local stiffness scales according to the eigenvalues of the $\mathbf{P}$ tensor. This method has been found

to provide the correct bulk elastic response in thin structures (in which free surfaces are important) and in bodies containing planar surfaces.

5. Direct numerical method

This section presents a summary of the numerical approximation to the peridynamic equations that is used in the EMU code [7]. The region is discretized into nodes, each with a known volume in the reference configuration. Taken together, the nodes form a grid. In EMU the method is mesh free in the sense that there are no elements or other geometrical connections between the nodes. However, in FEA the peridynamic grid becomes an assemblage of nonlinear trusses. For simplicity, the details of the method implemented in EMU are discussed here using the linearized version of the peridynamic theory applied to a homogeneous body. The discretized form of the equation of motion (1) replaces the integral by a finite sum

$$\rho\ddot{\mathbf{u}}_i^n = \sum_p \boldsymbol{f}(\mathbf{u}_p^n - \mathbf{u}_i^n, \mathbf{x}_p - \mathbf{x}_i)V_p + \mathbf{b}_i^n, \tag{22}$$

where $\boldsymbol{f}$ is given by Eq. (4), n is the time step number, and subscripts denote the node number, so that

$$\mathbf{u}_i^n = \mathbf{u}(\mathbf{x}_i, t^n). \tag{23}$$

In Eq. (22) V_p is the volume of node p, which for a uniform rectangular grid is simply Δx^3. The sum in Eq. (22) is taken over all nodes p such that $|\mathbf{x}_p - \mathbf{x}_i| < \delta$. The discretized equation of motion, Eq. (22), is easy to implement in its fully nonlinear form. However, for purposes of error analysis and numerical stability analysis, it is necessary to work with a linearized version. The discretized form of the linearized peridynamic model is

$$\rho\ddot{\mathbf{u}}_i^n = \sum_p \mathbf{C}(\mathbf{x}_p - \mathbf{x}_i)(\mathbf{u}_p^n - \mathbf{u}_i^n)V_p + \mathbf{b}_i^n, \tag{24}$$

where $\mathbf{C}$ is a tensor-valued function called the *micromodulus* defined by

$$\mathbf{C}(\boldsymbol{\xi}) = \frac{\partial \boldsymbol{f}}{\partial \boldsymbol{\eta}}(0, \boldsymbol{\xi}) \quad \forall \boldsymbol{\xi}. \tag{25}$$

Hence, the pairwise force in the linearized theory is given by $\boldsymbol{f} = \mathbf{C}(\boldsymbol{\xi})\boldsymbol{\eta}$. For the special case of proportional materials, it follows from Eqs. (14)–(16) in [4] and Eq. (25) that

$$\mathbf{C}(\boldsymbol{\xi}) = c\frac{\boldsymbol{\xi} \otimes \boldsymbol{\xi}}{|\boldsymbol{\xi}|^3} \quad \text{or} \quad C_{ij}(\boldsymbol{\xi}) = c\frac{\xi_i \xi_j}{(\xi_k \xi_k)^{3/2}}, \tag{26}$$

where the latter expression uses components in a Cartesian coordinate frame. An explicit central difference formula is used for acceleration in either Eq. (22) or Eq. (24)

$$\rho\ddot{\mathbf{u}}_i^n = \frac{\mathbf{u}_i^{n+1} - 2\mathbf{u}_i^n + \mathbf{u}_i^{n-1}}{\Delta t^2}. \tag{27}$$

Through the use of standard error analysis techniques [4], the spatial and temporal discretization errors associated with Eq. (24) can be shown to be $O(\Delta x^2) + O(\Delta t^2)$. In addition, von Neumann stability analysis [8] of Eq. (24) leads to a stable time step requirement of

$$\Delta t < \sqrt{\frac{2\rho}{\sum_p V_p |\mathbf{C}(\mathbf{x}_p - \mathbf{x}_i)|}}. \tag{28}$$

The value of the horizon δ may depend on the physical nature of the application being modeled. For example, at the nanoscale, δ would be determined by the distance over which physical interaction between atoms or molecules occurs. However, in macroscale calculations, δ can be chosen according to convenience, since, as shown previously, the parameters such as c that determine the bulk elastic properties of the material can be fitted to experimental data for any value of δ. See, for example, Eq. (10). In practice, for macroscale modeling, the value $\delta = 3\Delta x$ usually works well. Values much smaller than this typically result in undesirable grid effects (cracks grow along the rows or columns of the grid). Values much larger than this may result in excessive wave dispersion and require very large computer run times.

Boundary conditions are somewhat different in the peridynamic method than in the classical theory. As shown in [1], the variational formulation of the peridynamic equations does not lead to natural boundary conditions, which in the classical theory are traction boundary conditions. Instead, forces at the surface of a body must be applied as body forces $\mathbf{b}$ within some layer under the surface. In practice, this layer usually has thickness δ. Similarly, displacement boundary conditions must be prescribed within a layer of finite thickness under the surface.

Although the above analysis assumes a regular lattice of nodes, the method is not restricted to such structured grids. Through the use of irregular grids, complex geometries may be modeled, and the full advantages of a meshless method are realized.

6. Finite element implementation

Recall that the interaction between the particles of a peridynamic continuum occurs through bonds that represent the physical force between pairs of particles. The totality of all such bonds forms a network within a body that connects all pairs of particles that interact with each other. Such a network of the bonds is Lagrangian in the sense that the bonds are defined in the reference (undeformed) configuration; therefore, the connectivity does not change during deformation.

Although the discretization in EMU described in the previous section is meshless, for purposes of implementation in a finite element code, a mesh made of truss elements with the appropriate stiffness properties is used to represent the peridynamic bonds. To do this, first observe that multiplying Eq. (22) by V_i leads to an equation of motion identical in form to that of FEA:

$$V_i\rho\ddot{\mathbf{u}}_i^n = \sum_p \boldsymbol{f}(\mathbf{u}_p^n - \mathbf{u}_i^n, \mathbf{x}_p - \mathbf{x}_i)V_p V_i + \mathbf{b}_i^n V_i, \tag{29}$$

or

$$\mathbf{M}\ddot{\mathbf{u}}^n + \mathbf{F}_T^n = \mathbf{F}_e^n, \tag{30}$$

where $\mathbf{M}$ is the lumped mass matrix, $\mathbf{F}_e^n$ is the external force vector, and $\mathbf{F}_T^n$ is the internal force vector. Each diagonal term of $\mathbf{M}$ is ρV_i and each component of $\mathbf{F}_e^n$ is $\mathbf{b}_i^n V_i$. Likewise, each component of $\mathbf{F}_T^n$ is $\sum_p \boldsymbol{f}(\mathbf{u}_p^n - \mathbf{u}_i^n, \mathbf{x}_p - \mathbf{x}_i) V_p V_i$, which is the sum of all the forces from the trusses connected to node i. Thus, the process of implementing peridynamics in an FEA code essentially boils down to a preprocessing task of generating a truss assembly (mesh) and stiffness properties for the trusses consistent with the peridynamic theory.

Although there are no technical issues with generating irregular peridynamic truss meshes, for simplicity only uniform rectangular meshes were used for the simulations presented in this paper. In this case a uniform rectangular array of nodes is first defined, and then trusses are generated by connecting any given node i to any other node p that lies within a sphere of radius δ centered at node i. Through the use of $\delta = 3\Delta x$, approximately 114 trusses are connected to each interior node of a three-dimensional body. Clearly, for even moderate-size problems, millions of trusses may be necessary if the entire region is modeled as peridynamic.

To alleviate some of the computational burden, it would be very desirable to couple a peridynamic truss mesh to a conventional FEA mesh. In this way, peridynamics could be used for the subregions where damage or fracture is expected, and the more efficient conventional FEA could be used for the remainder of the structure. Unfortunately, this coupling is not as simple as sharing nodes between meshes, as is commonly done in FEA. As previously mentioned, the boundaries in peridynamics are "fuzzy" (prescribed displacements or loads must be applied through a finite volume rather than on a surface). Thus, the coupling must be done over a region that spans some thickness, typically taken to be δ, from the exterior surface. This is most conveniently done by introducing a displacement constraint between the boundary of the peridynamic mesh and the FEA mesh boundary. If p denotes nodes within a distance δ of the peridynamic/conventional boundary, and h denotes the FEA nodes or elements to which they will be coupled, then the constraint is

$$\mathbf{u}_p = \mathbf{N}(a, b, c)\mathbf{u}_h, \tag{31}$$

where (a, b, c) are the parametric coordinates of the p nodes within or extrapolated from the h elements, and $\mathbf{N}$ is the shape function matrix for the h elements. The constraint defined by Eq. (31) effectively enforces continuity of strain between the peridynamic mesh and the conventional FEA mesh. Since many general-purpose FEA codes permit constraint equations, Eq. (31) may be directly input, although the amount of data may be voluminous.

A more convenient way to couple the peridynamic and conventional parts of the FEA mesh is with embedded nodes and elements, which are available in the commercial general purpose ABAQUS/Explicit computer code [9]. This capability makes the imposition of the constraint much easier. To use the embedded element feature, a band of thickness δ containing conventional continuum elements is defined to overlap the peridynamic trusses. The trusses are then specified to be embedded in the continuum elements. To keep the overlap region from being too stiff, the elastic modulus and density for the host continuum elements are set to very small values.

The definition of section and material properties for the peridynamic trusses is again a straightforward application of the theory. The mass of the nodes is defined via lumped masses as ρV_i, and the truss densities are set to zero. Because Eqs. (29) and (30) indicate that only the forces from the trusses connected to a given node are required, there is some nonuniqueness in the definition of the cross-sectional area A and elastic modulus E for the trusses. A convenient separation, which preserves the conventional units of these properties, is

$$A = (V_p V_i)^{1/3}, \quad E = c(V_p V_i)^{2/3}. \tag{32}$$

For a uniform rectangular mesh, then

$$A = \Delta x^2, \quad E = c\Delta x^4. \tag{33}$$

Also, as shown by Eq. (6), the bond stretch s is identical to the engineering strain in the trusses, thus the fracture strain of the trusses is

$$\epsilon_f = s_0. \tag{34}$$

For elastic–plastic materials, Eq. (16) with the inherent Poisson's ratio of $\frac{1}{4}$ indicates that the strain s_y at which the bonds or trusses yield is related to Young's modulus E and the engineering ultimate stress in tension σ_{ult} by

$$s_y \approx \frac{\boldsymbol{\sigma}_{ult}}{2E}. \tag{35}$$

For implementation in FEA, we set the truss element yield strain to $\varepsilon_y = s_y$ as determined by Eq. (35).

In contrast to EMU, in the current FEA implementation, the short-range forces are also restricted to the region within one horizon of each node. Thus, the contact interactions of Eqs. (17)–(19) are a simple modification of the compressive behavior of the trusses. For convenience this was implemented with a user-defined material in ABAQUS. More general application of the short-range forces consistent with EMU might be accomplished by a node-to-node contact algorithm. Unfortunately, this feature is not currently available in ABAQUS.

To complete the FEA model generation, the elastic modulus of the trusses that are within a distance δ of free surfaces needs to be modified by a normalization factor derived from Eq. (21). From Eqs. (21) and (32), the elastic modulus $E_b(\mathbf{X})$ of an element near a boundary is

$$E_b(\mathbf{X}) = \frac{p_\infty^1}{p_\infty^1(\mathbf{X})} E. \tag{36}$$

For convenience of input into ABAQUS, we chose to capture this modulus variation near free surfaces with node-based, user-defined field variables.

7. Example problems

Three example problems that span a reasonably broad range of structural responses were chosen to demonstrate the equivalency of the FEA implementation with the direct implementation contained in the EMU code. Although as stated earlier

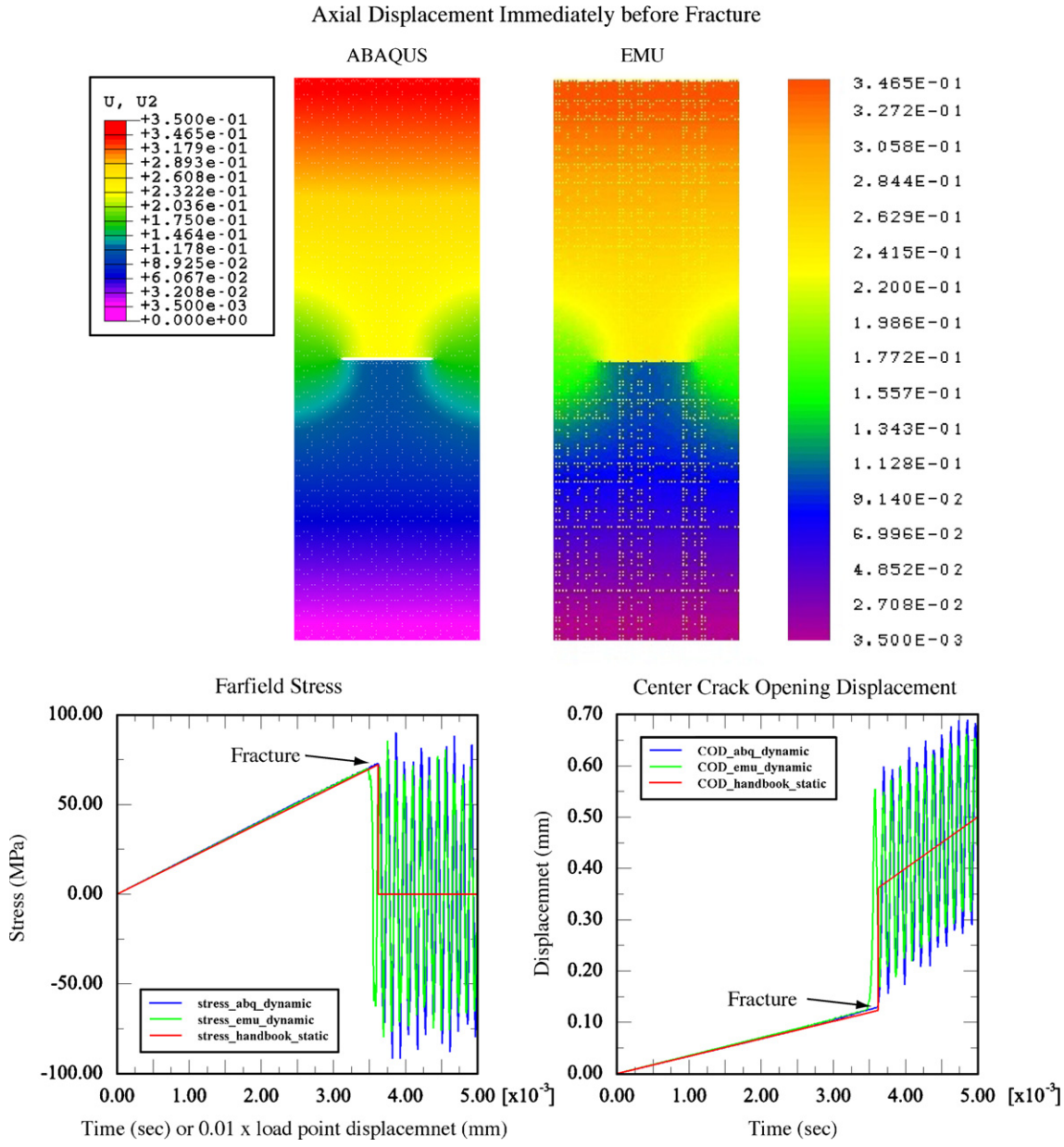

Fig. 1. Deformation and response histories for the center cracked plate example.

the goal of this work is to demonstrate that peridynamics can be easily implemented with FEA rather than validation of the peridynamic theory, the examples do provide some insight into the accuracy and capability of peridynamics for challenging simulations that an analyst might face. To effect meaningful comparisons, all problems were run in EMU and ABAQUS with the same uniform peridynamic grid and the same solution time step on a single processor of an SGI Altix 350 computer (1.5 GHz Intel Itanium 2 processor with 20 GB RAM).

7.1. Brittle center cracked plate

The first example, a classical fracture mechanics problem, is a brittle center cracked plate under a tensile load. The plate is 100 mm wide by 300 mm long by 10 mm thick, with an existing 50 mm through-thickness crack perpendicular to the long axis. The grid spacing is 2 mm, resulting in 37,500 nodes and approximately 1,700,000 trusses in ABAQUS. The material is aluminum with an elastic modulus of 68,900 MPa, a density of 2.7 g/cc, and a fracture toughness of 24 MPa $m^{1/2}$. Using the brittle microelastic model, the fracture toughness was converted to the fracture strain for each truss from Eq. (11). A prescribed displacement end load was ramped up over 5 ms to ensure quasi-static response before fracture. Fig. 1 compares the center crack opening displacement and the far-field stress to the static handbook [10] solution and EMU. As is evident, both numerical implementations of peridynamics are within a few percent of the handbook solutions for the crack opening displacement and the stress at fracture. It is interesting to note that there are some bond failures (as evidenced by the

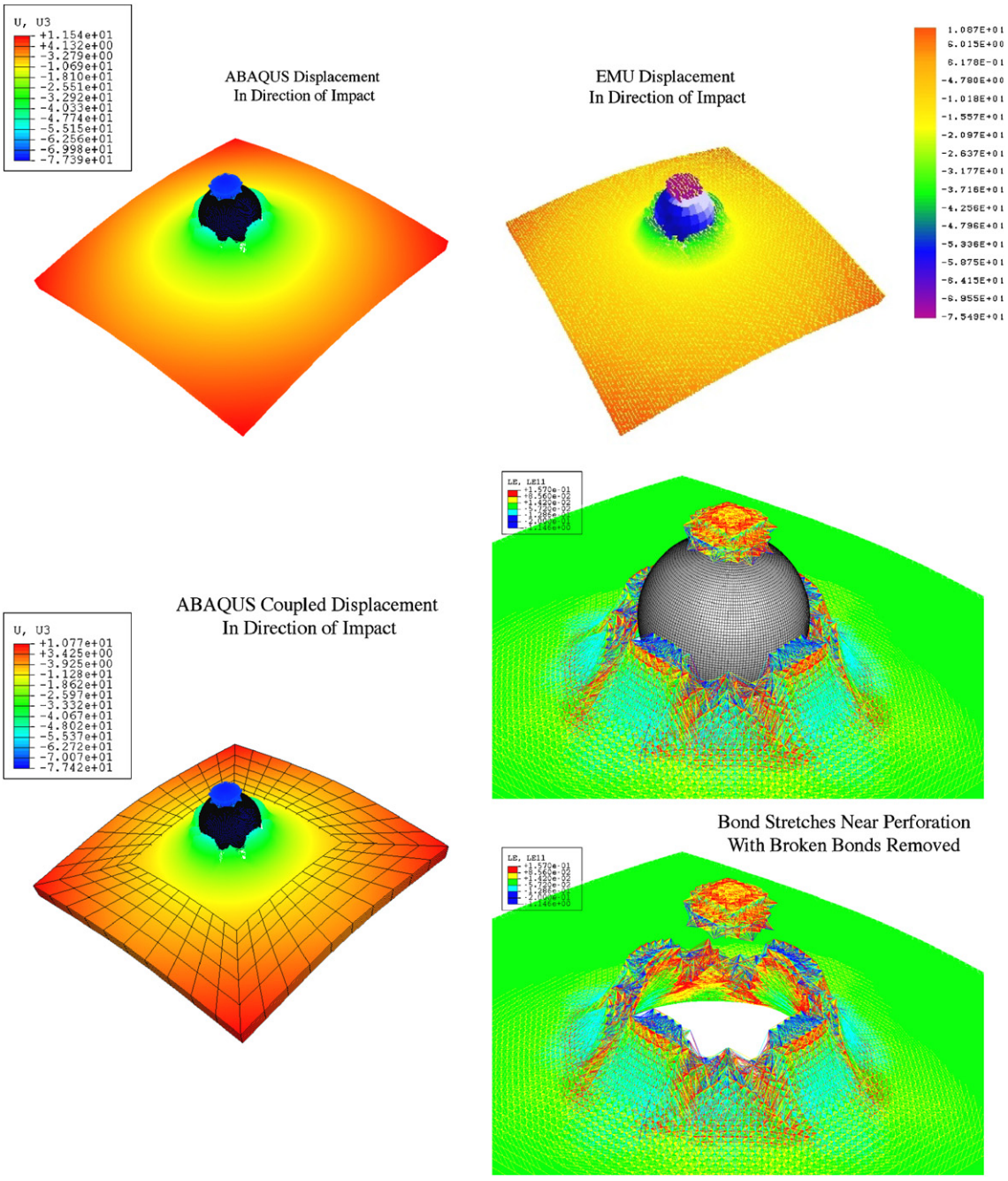

Fig. 2. Deformations for the plate perforation example.

low-amplitude, high-frequency load oscillation) before fracture or unstable extension of the crack.

Detailed stress or strain contours are not shown since these are not intrinsic variables in the peridynamic theory. Although not currently implemented, a number of techniques have been proposed to recover these fields from peridynamic solutions. For stress recovery direct force projection, bond force averaging and internal energy differentiation techniques seem promising while straightforward displacement field interpolation with spatial differentiation or bond stretch averaging may suffice for strain recovery.

7.2. *Plate perforation*

The second example is that of a rigid spherical ball impacting a ductile aluminum plate. The 5.11 kg ball is 50 mm in diameter, and the square plate is 250 mm on each side by 12.5 mm thick. The aluminum has a Young's modulus of 68,900 MPa, a density of 2.7 g/cc, and an ultimate strength of 310 MPa at 17% strain. Using Eq. (35) the ultimate strength was converted to the yield stretch for the microplastic model and the strain at the ultimate strength was used for the fracture stretch. The grid spacing is 2.5 mm, resulting in 50,000 nodes and approximately 2,400,000

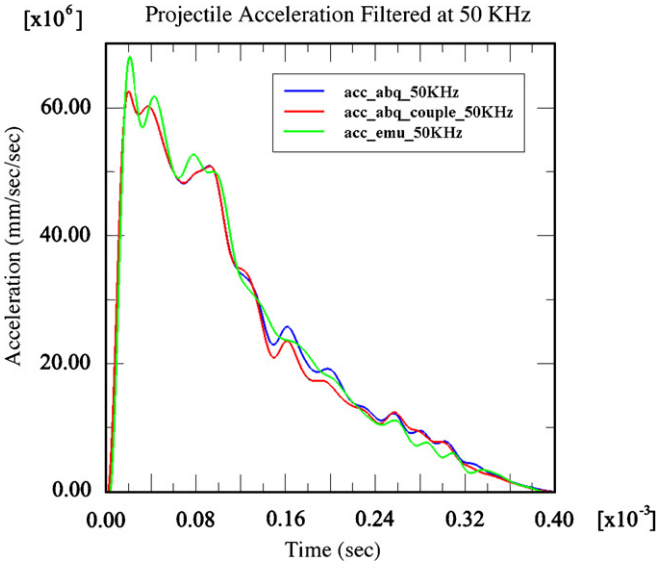

Fig. 3. Projectile accelerations for the plate perforation example.

trusses in ABAQUS. The sphere impacts normal to the plate at its center with a velocity of 500 m/s.

In addition to a fully peridynamic FEA model of the plate, this example was also simulated using the coupled conventional/peridynamic FEA method described near Eq. (31). In the coupled model, the outer three-fourths of the plate consisted of 8-node reduced integration continuum elements. With this representation, there are 1200 conventional continuum elements, in addition to 12,500 peridynamic nodes and approximately 670,000 trusses. Thus, the coupled procedure greatly reduces the number of nodes and elements compared with the fully peridynamic FEA model.

Interaction between the spherical projectile and the plate is modeled using a kinematic contact algorithm. Fig. 2 shows the deformations shortly after the ball perforated the plate and Fig. 3 shows the acceleration history of the ball. Although there is no analytical solution to this problem, the plug formation and petaling are well documented, experimentally observed features of this type of impact event [11]. The comparisons of FEA to EMU in both deformation and acceleration are within a few percent of each other, and there is very little difference (except in run times) using the mesh coupling technique.

7.3. Projectile penetration

The final example is that of a rigid projectile penetrating a cube of metal. From a model size and deformation viewpoint this was the most taxing of the three examples. Indeed, the ABAQUS preprocessor effectively limited the model to around five million trusses. The aluminum target was a 400 mm cube. The aluminum had the same properties as in the perforation example. The grid spacing of 10 mm resulted in 64,000 nodes and approximately 5,000,000 trusses in ABAQUS. Because large motion of the particles was anticipated, a limited number of additional compression-only trusses were added to the nodes in the path of the penetrator to permit short-force interaction outside of the horizon. The penetrator was 100 mm in diameter and 300 mm long, with a 3 CRH (caliber radius head) ogive nose. The penetrator mass was 15 kg, and it impacted the target at 700 m/sec. Again, interaction between the projectile and the target was captured with a kinematic contact algorithm. EMU accounts for the node radii in the contract algorithm for this type of projectile, so that for purposes of the contact algorithm for a rigid penetrator in EMU, each node acts like a hard sphere. Since the ABAQUS code does not account for a node radius, the dimensions of the projectile are increased by the diameter of the nodes (the grid spacing) in the FEA simulations to compensate for this. Fig. 4 compares the resulting deformations and acceleration of the penetrator. Here, the peak penetrator accelerations predicted by EMU and FEA are again within a few percent, although there is a slight difference in the character of the penetrator acceleration history and the target deformation. A few parametric studies where the number of additional trusses for the short-range forces was varied indicate that these differences may be due to the limited span of the short-range forces in the FEA implementation. Also the lack of node radii in the FEA contact may be a contributing factor.

It is noted that in both this and the previous examples, the peridynamic FEA simulations never suffered from any of the numerical problems (mesh entanglement, advection anomalies, etc.) that one might expect with conventional (partial differential equation) continuum mechanics approaches. (Since EMU is meshless, the issue of mesh entanglement does not arise.) Freedom from these types of pathological behavior appears to be a key advantage of our approach.

As the examples demonstrate, there are no substantial differences in results between the direct and FEA implementations of peridynamics, although there appear to be some significant differences in computational efficiency. Table 1 compares computer wall-clock run times between the direct meshless and FEA simulations. It is noted that these run times are measured with no competition with other jobs, i.e., no other jobs were running on the processor during the time that EMU or ABAQUS was executing. As is evident, the FEA (ABAQUS) implementation is dramatically faster than the direct meshless approach (EMU). On the other hand, even though the memory usage could not be precisely quantified it appears that EMU is almost an order of magnitude less demanding of physical memory than ABAQUS in most cases. Since both codes use a lumped mass central difference explicit equation of motion solver, the most likely explanation for the speed differences is the fact that EMU is meshless and ABAQUS uses a predefined mesh. EMU searches the domain every time step to determine which nodes interact whereas in the FEA approach the nodes that interact are determined once by the mesh generator at the start of the analysis. In essence EMU generates a new mesh every time step where the FEA approach does this once. Depending on the extent and complexity of the domain the time spent in searching or mesh generation can be significant. Furthermore, because these explicit codes do not factor any matrices the time spent in the solver is usually dwarfed by the time spent doing element force calculations. Thus, even if there were some differences

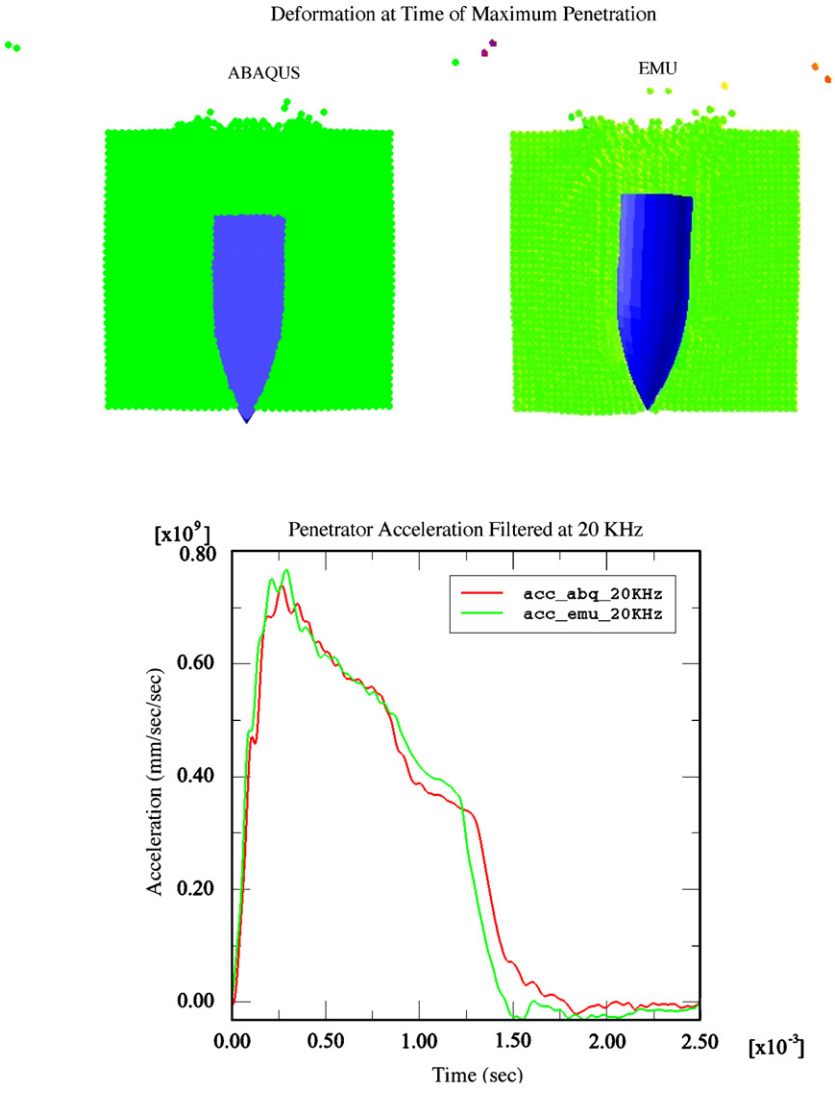

Fig. 4. Deformations and projectile acceleration for the projectile penetration example.

Table 1
Computer run-time comparisons on a single processor of an SGI Prism 350 computer

Example problem	Approximate model size (nodes/elements)	Solution time step (μs)	Wall-clock run times (min)	
			EMU	ABAQUS
Center cracked plate	37,500/1,700,000	0.25	2255	350
Plate perforation	50,000/2,400,000	0.20	283	73
Plate perforation (coupled)	12,500/670,000	0.20	–	27
Cube penetration	64,000/5,000,000	0.50	1328	294

in the solver these would not appreciably affect the overall solution time. The differences in memory usage may also be due to the meshless versus mesh architecture of the two codes. It is the authors' understanding that ABAQUS/Explicit stores the mesh (element connectivity) and associated variables in core or short term memory whereas noted above EMU regenerates the connectivity. Thus, one would expect that EMU would use considerably less memory. There are probably other factors that contributed to these differences, however, the proprietary nature of the ABAQUS code prevented the authors from fully exploring them.

8. Conclusions

The theoretical basis for peridynamics together with the numerical implementations and examples presented in this paper show the potential that this approach has for problems involving damage and fracture although complete validation of the

theory is an ongoing process that may take many years. A key advantage of the peridynamic approach is its ability to model individual cracks that grow and interact with each other in arbitrarily complex patterns. The method is designed to reproduce a prescribed energy release rate that is characteristic of the material in which a crack is growing. It is also applicable to interface fractures.

Numerical implementation of the peridynamic equations leads to the meshless method used in the EMU code. However, since we have shown that the technique can easily be adapted and coupled to conventional finite element analysis with no loss of computational efficiency (and perhaps with some significant speed gains), a much broader range of structural problems is now within the reach of the practicing engineering analyst. Furthermore, given the ubiquitousness of FEA the adaptation described in this paper may expedite the validation of the peridynamic theory. We have also demonstrated that the resulting FEA implementation of peridynamics in the ABAQUS code leads to essentially the same results as EMU in problems in which both methods are applicable. As demonstrated here, an FEA model can include both a peridynamic and conventional finite element subregions whose boundary is conveniently set up using embedded elements.

The FEA implementation of peridynamics is expected to be especially useful in penetration modeling because it avoids many of the well-known difficulties in describing the interface between a penetrator and a target when using conventional finite elements. In particular, the use of truss elements to describe the target is expected to reduce or eliminate problems with mesh tangling and distortion.

Acknowledgments

This work was supported by the United States Department of Energy and by the Joint US DOE/DoD Munitions Technology Program. Sandia is a multiprogram laboratory operated by Sandia Corporation for the United States Department of Energy under contract DE-AC04094AL85000.

References

[1] S.A. Silling, Reformulation of elasticity theory for discontinuities and long-range forces, J. Mech. Phys. Solids 48 (2000) 175–209.
[2] S.A. Silling, M. Zimmermann, R. Abeyaratne, Deformation of a peridynamic bar, J. Elasticity 73 (2003) 173–190.
[3] S.A. Silling, E. Askari, Peridynamic modeling of impact damage, in: F.J. Moody (Ed.), Problems Involving Thermal-Hydraulics, Liquid Sloshing, and Extreme Loads on Structures, American Society of Mechanical Engineers, New York, 2004, PVP-vol. 489, pp. 197–205.
[4] S.A. Silling, E. Askari, A meshfree method based on the peridynamic model of solid mechanics, Comput. Struct. 83 (2005) 1526–1535.
[5] S.A. Silling, F. Bobaru, Peridynamic modeling of membranes and fibers, Int. J. Non-Linear Mech. 40 (2005) 395–409.
[6] O. Weckner, R. Abeyaratne, The effect of long-range forces on the dynamics of a bar, J. Mech. Phys. Solids 53 (2005) 705–728.
[7] EMU website, www.sandia.gov/emu/emu.htm.
[8] L. Lapidus, G.F. Pinder, Numerical Solution of Partial Differential Equations in Science and Engineering, Wiley, New York, 1982 p. 171.
[9] ABAQUS/Explicit Version 6.6 User's Manual, ABAQUS Inc., Providence, Rhode Island, 2006.
[10] H. Tada, The Stress Analysis of Cracks Handbook, Del Research Corporation, St. Louis, 1973, pp. 2.1–2.3.
[11] W. Johnson, Impact Strength of Materials, Edward Arnold, London, 1972, pp. 138–146, 330–336.